23. Schmidt, J. V., Matteson, P. G., Jones, B. K., Guan, X. J. & Tilghman, S. M. The Dlk1 and Gtl2 genes are linked and reciprocally imprinted. *Genes Dev.* **14,** 1997–2002 (2000).
24. Kobayashi, S. *et al.* Mouse Peg9/Dlk1 and human PEG9/DLK1 are paternally expressed imprinted genes closely located to the maternally expressed imprinted genes: mouse Meg3/Gtl2 and human MEG3. *Genes Cells* **5,** 1029–1037 (2000).
25. Lin, S. P. *et al.* Asymmetric regulation of imprinting on the maternal and paternal chromosomes at the Dlk1-Gtl2 imprinted cluster on mouse chromosome 12. *Nature Genet.* **35,** 97–102 (2003).
26. Georgiades, P., Watkins, M., Surani, M. A. & Ferguson-Smith, A. C. Parental origin-specific developmental defects in mice with uniparental disomy for chromosome 12. *Development* **127,** 4719–4728 (2000).
27. Georgiades, P., Watkins, M., Burton, G. J. & Ferguson-Smith, A. C. Roles for genomic imprinting and the zygotic genome in placental development. *Proc. Natl Acad. Sci. USA* **98,** 4522–4527 (2001).
28. Moore, T. & Haig, D. Genomic imprinting in mamalian development: a parental tug-of-war. *Trends Genet.* **7,** 45–49 (1991).
29. Reik, W. & Walter, J. Genomic imprinting: parental influence on the genome. *Nature Rev. Genet.* **2,** 21–32 (2001).
30. Murphy, S. K. & Jirtle, R. L. Imprinting evolution and the price of silence. *BioEssays* **25,** 577–588 (2003).

Supplementary Information accompanies the paper on **www.nature.com/nature**.

Acknowledgements We thank A. Surani, Wellcome CRC Institute, J. Carroll, University College London and T. Moore, University College Cork, Ireland, for critical reading and discussions; O.-Y. Kwon, MacroGen, for microarray analysis; and T. Kumagai for technical assistance. This work was supported by grants from the Bio-oriented Technology Research Advancement Institution (BRAIN), Japan, and The Ministry of Education, Science, Culture and Sports of Japan.

Competing interests statement The authors declare that they have no competing financial interests.

Correspondence and requests for materials should be addressed to T.K. (tomohiro@nodai.ac.jp).

Intracellular gate opening in Shaker K^+ channels defined by high-affinity metal bridges

Sarah M. Webster*, Donato del Camino*, John P. Dekker & Gary Yellen

Department of Neurobiology, Harvard Medical School, 220 Longwood Avenue, Boston, Massachusetts 02115, USA

* These authors contributed equally to this work

Voltage-gated potassium channels such as Shaker help to control electrical signalling in neurons by regulating the passage of K^+ across cell membranes. Ion flow is controlled by a voltage-dependent gate at the intracellular side of the pore, formed by the crossing of four α-helices—the inner-pore helices. The prevailing model of gating is based on a comparison of the crystal structures of two bacterial channels—KcsA in a closed state and MthK in an open state—and proposes a hinge motion at a conserved glycine that splays the inner-pore helices wide open[1]. We show here that two types of intersubunit metal bridge, involving cysteines placed near the bundle crossing, can occur simultaneously in the open state. These bridges provide constraints on the open Shaker channel structure, and on the degree of movement upon opening. We conclude that, unlike predictions from the structure of MthK, the inner-pore helices of Shaker probably maintain the KcsA-like bundle-crossing motif in the open state, with a bend in this region at the conserved proline motif (Pro-X-Pro) not found in the bacterial channels. A narrower opening of the bundle crossing in Shaker K^+ channels may help to explain why Shaker has an approximately tenfold lower conductance than its bacterial relatives.

The recent elucidation of four K^+ channel crystal structures has revealed the general architectural motifs in this large family of transmembrane proteins[1–5]. Each of the tetrameric structures has a central pore formed by two transmembrane helices and a selectivity filter structure from each of the four subunits. The sequence homology in the family of K^+ channels is strongest in the region of the selectivity filter, a region that is crucial for allowing rapid and selective permeation of K^+ ions[6]. Structurally, the selectivity filter is nearly identical in the channels solved thus far. However, the structures reveal significant differences in the conformation of the inner-pore helices in the region of the intracellular gate.

On the basis of differences in inner-helix configuration between two types of bacterial K^+ channels, KcsA and MthK[1,2,5], MacKinnon and colleagues proposed a general model of K^+ channel gating. In the apparently closed KcsA structure, the inner M2 helices are straight, and they cross in the lower part of the S6 to form an inverted teepee-like structure. Access from the intracellular surface to the pore is through a long, narrow, hydrophobic entrance. MthK, by contrast, was crystallized in conditions that favoured the open state of the channel. The inner helices are bent at Gly 83, which splays them apart to form a wide inner pore, 12 Å across at its narrowest point. These two structures are proposed to represent the closed and open states. In the gating model, the inner helices would swing around the conserved glycine to move from the narrow, closed KcsA pore to the wide, open MthK pore. This structure-based gating model is appealing in its simplicity, but it does not fit with the details of functional experiments done on voltage-gated K^+ channels. Here we present a model of gating for a voltage-dependent K^+ channel based on constraints established by the state dependence of metal bridging at two engineered binding sites.

A cysteine replacement at Shaker V476 creates a high-affinity Cd^{2+}-binding site that stabilizes an open state of the channel[7]. Cd^{2+} binding prevents these channels from closing even at very negative voltages, apparently by forming a bridge between a cysteine in one subunit and a native histidine (H486) in a neighbouring subunit[7] (Fig. 1). Replacement of the native histidine with tyrosine, threonine or valine abolished this high-affinity Cd^{2+} 'lock-open effect'. Other ligand combinations (Cys–Cys, His–Cys, His–His)

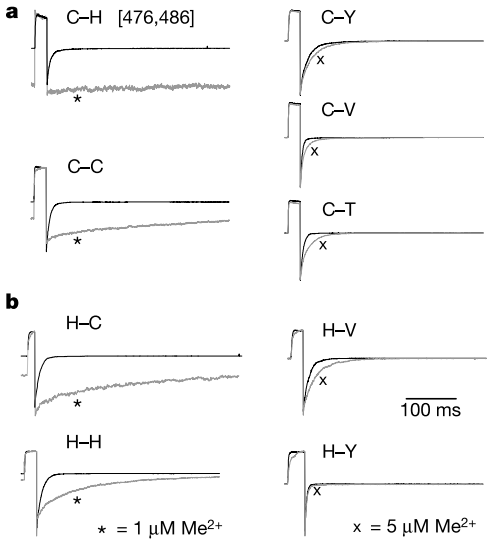

Figure 1 The lock-open effect requires metal binding residues at positions 476 and 486. Channel currents measured in control solutions (black traces) or in the presence of **a**, Cd^{2+} or **b**, Zn^{2+} (grey traces). Lock-open (prevention or delay of closure) occurs only for channels with two metal-binding ligands (left column), whereas channels with only one metal-binding ligand (right column) show only a slight slowing of the tails. Activating steps to +60 mV were followed by closure at −110 mV (C–C, C–H, C–V and C–T), −140 mV (H–C, H–H, H–V and C–Y) or −180 mV (H–Y). Without metal, maximum outward currents ranged from 0.7 to 2.7 nA; with metal, outward currents (normalized in the figure) ranged from 15 to 37% of the control because of inactivation.

could also stabilize the open state, although they were not quite as effective as the original Cys–His bridge. The Cd^{2+} lock-open effect requires specific metal-binding ligands, either cysteine or histidine, at both positions, 476 and 486, confirming that Cd^{2+} forms a bridge between these two positions.

This metal bridge can be used as a constraint on the open-state structure only if it does not distort the open state substantially. We used the binding of three open-channel blockers—tetraethylammonium (TEA), tetrabutylammonium (TBuA) and the inactivation ball peptide (EBP)[8]—as one test for distortion of the open state, by comparing the affinity of the blockers for both the normal open state and the locked-open state. The blockers were applied by fast perfusion switching during a long open pulse either before or after the channel was locked open (Fig. 2a). For each of the blockers, the affinity was slightly better for locked-open channels than for channels in the absence of Cd^{2+} (fold increase: TEA, 2.6 ± 0.5; TBuA, 2.2 ± 0.5; EBP, 4.0 ± 1.1). The structural changes produced by locking the channel open did not change blocker binding much (and actually slightly enhanced the binding). These changes correspond to a change in binding energy of only about 0.8–1.4 kT, and are smaller than the ~2.3 kT change in TEA affinity produced by removing four methylene groups in the T441S mutant[9].

Many amino-acid substitutions in this region of the S6 affect the single-channel conductance by up to about fourfold[10,11], so it seems reasonable to use single-channel conductance as another test for distortion of the open state by the metal bridge. The single-channel current of V476C channels was not significantly different when the channel was locked open (Fig. 2b). The ratio of the single-channel current at 0 mV with and without 50 μM Cd^{2+} is 1.08 ± 0.12 ($n = 6$). As in the case with blocker affinity, this small change suggests that the bridge does not drastically alter the open state. A model of the open state should therefore be able to accommodate a metal bridge between V476C and H486 without much distortion.

At a second engineered site, V474C (at the position of the V in the conserved Pro-Val-Pro), Cd^{2+} binds to multiple cysteines and blocks the current nearly irreversibly[12]. Channels with only two cysteines at V474C bind Cd^{2+} reversibly, suggesting that the irreversible binding seen in a channel with four cysteines is due to the direct binding of three or four centrally facing cysteines. To achieve such tight binding, the sulphydryl groups of the cysteine side chains must come into close proximity to coordinate a single Cd^{2+} ion jointly. A large change in the distance between these ligands upon channel opening, such as the change envisioned by the KcsA/MthK gating model, would predict state-dependent binding at this position, and Cd^{2+} binding should strongly influence the gating equilibrium.

To test this prediction, it was necessary to simplify the normally complex, multi-step process of gating. To accomplish this goal, these studies were conducted in a mutant background that separates the voltage range of channel opening from that of the multi-step voltage sensor movement. This background contains three conservative mutations of uncharged residues in the S4 helix: V369I, I372L and S376T (ILT)[13–15]. We introduced the V474C mutation into the ILT background (ILT 474C) and confirmed that it maintained the essential hallmarks of the ILT two-state model: voltage separation of the major charge movement and channel opening, a reduced slope and positive-shifted midpoint of the gating curve, and single exponential opening kinetics after a short delay (data not shown).

Because V474C channels do not conduct current when Cd^{2+} is bound, the gating equilibrium of Cd^{2+}-bound channels cannot be measured directly. However, the release of Cd^{2+} in the presence of a dithiol reagent, 2,3-dimercaptopropanesulphonate (DMPS), is steeply voltage dependent (in both the ILT and WT[12] backgrounds) in a way that suggests that Cd^{2+}-bound channels still have voltage-dependent opening, with release occurring only from the open state. Therefore, the gating of Cd^{2+}-bound channels was inferred from the voltage dependence of recovery. In 0.5 mM DMPS, the recovery rates of ILT 474C had a voltage dependence similar to that of gating

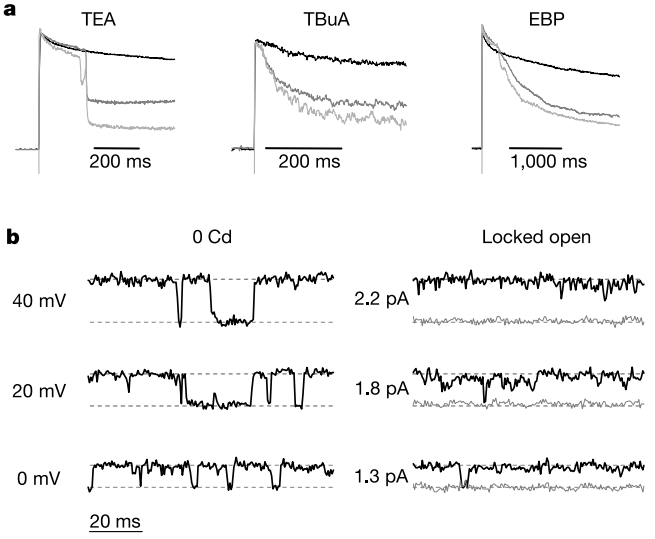

Figure 2 The blocker affinity and single-channel conductance of the locked-open state are similar to those of the normal open state. **a**, Open channel blockers applied in the middle of a step to 0 mV give nearly the same block whether the channel is open (dark grey) or locked open (with prior exposure of 10 μM Cd^{2+}, light grey; no blocker, black). Blocker concentrations: TEA, 1 mM; TBuA, 25 μM; EBP, 0.4 μM. Control currents ranged from 0.2 to 1 nA; with metal, outward currents (normalized in the figure) ranged from 42% to 80% of control because of inactivation. **b**, Single-channel recordings from 476C channels in 0 μM Cd^{2+} (left) and 50 μM Cd^{2+} (right). Dotted lines show open and closed levels; the light grey trace shows the closed level in a subsequent pulse where the channel had inactivated.

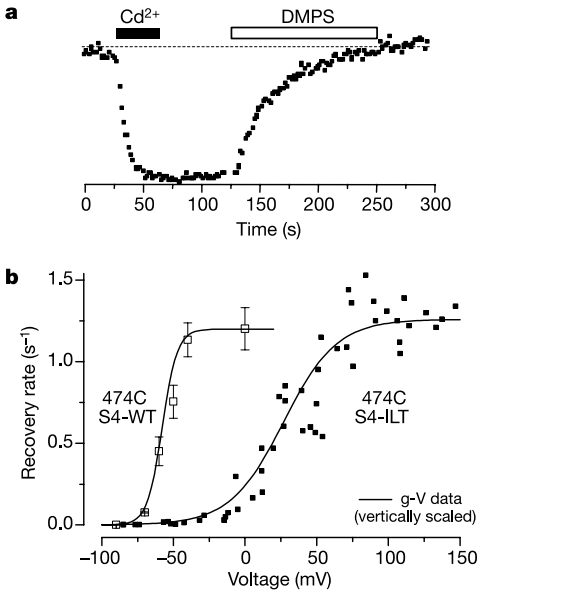

Figure 3 The recovery of ILT V474C channels from Cd^{2+} blockade suggests that cadmium has little effect on the open/closed equilibrium of bound channels. **a**, Recovery was measured by pulsing (+120 mV for 40 ms from −90 mV) in the presence of 0.5 mM DMPS (squares, current for each pulse; dotted line, 700 pA). **b**, The recovery rate of ILT V474C from Cd^{2+} block as a function of voltage with 0.5 mM DMPS (filled squares). The Cd^{2+} recovery rate for WT 474C from ref. 12 (open squares ± s.e.m.) and the corresponding g-Vs (line with vertical scaling to the recovery rates) are plotted for comparison.

in ILT V474C (Fig. 3). This agrees with the earlier result in a wild-type S4 background[12] (Fig. 3b), which has more complicated gating. Although the ILT mutation shifts the voltage dependence by over 90 mV and makes it much shallower, the voltage dependence of Cd^{2+}-free gating (the g-V) agrees with that for Cd^{2+} recovery in both cases. This, and the agreement between the maximal rate of recovery in the two mutants, makes a strong case for recovery occurring only from the open state, and that the open–closed equilibrium is not altered by Cd^{2+} binding. The relative lack of effect on the gating equilibrium suggests that Cd^{2+} is bound almost equally well in the open and closed states, suggesting that there is little change in the positions of the side chains of V474C with opening.

In two separate sets of experiments, we have shown that the two different metal bridges, V474C and V476C–H486, each occur with high affinity in the open state. We reasoned that if neither metal binding event distorted the open-state structure, then Cd^{2+} should bind both sites simultaneously in the open state. To test this prediction, we measured the ability of the double mutant V474C–V476C to bind Cd^{2+} at V474C after being locked open at V476C–H486 (Fig. 4). The channels were first locked open by a 380 ms application of Cd^{2+} to the intracellular surface of the channel, with a pore blocker (hexyltriethylammonium; C_6-TEA) present to protect V474C from modification. This treatment produced a clear lock-open effect, as shown by the sustained inward current during the negative test pulses. When the locked-open channels were exposed a second time to Cd^{2+}, there was rapid block at V474C (the rate constant was $3.9 \pm 0.2 \times 10^5\,M^{-1}\,s^{-1}$, $n = 3$, see Methods). This on rate for the block at V474C was about sevenfold slower than in a non-locked-open channel[16], but given the precise distance and geometry constraints required for Cd^{2+} binding to multiple cysteines, it does not seem surprising that even a small structural change produces a change in the on rate. We know that the equilibrium binding of Cd^{2+} to 474C remains very strong—essentially irreversible—even when the binding occurs with the channels locked open. Despite this change in kinetics, it appears that bridges for both the lock-open effect and for blockade can be accommodated simultaneously by the open state.

Both of the metal-binding bridges that we observe in the open state of Shaker are incompatible with the MthK-derived open-state model. By comparison with known structures with Cys–Cd^{2+}–Cys bridges (Cys-C_β to Cys-C_β of 4.0–6.9 Å, for example, in PDB 1D66), the β carbons in MthK that are equivalent to the 474C–Cd^{2+}–474C bridges are 5–12 Å too far apart (Fig. 5a, b, right). A similar analysis for the intersubunit 476C–Cd^{2+}–H486 positions estimates that these positions in MthK are ~10–15 Å more distant than required.

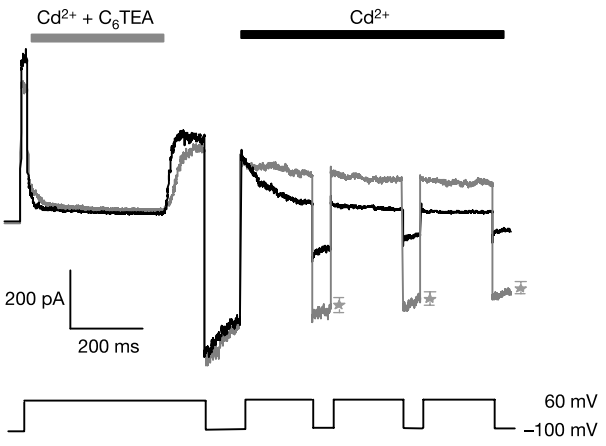

Figure 4 Cadmium ions can simultaneously bind V474C and bridge V476C–H486. 2 mM C_6-TEA was added to protect 474C while 40 μM Cd^{2+} is applied to lock the channels open (grey bar). Sustained inward current at negative pulses shows the extent of the lock-open effect (control, grey trace; stars, the mean current in control (±s.e.m., $n = 3$); black line, voltage protocol). The decay of current at negative voltages during a second application of Cd^{2+} (black bar, black trace) monitors binding to V474C.

Are these interactions actually occurring in the open state? Our use of the Shaker ILT mutation makes channel gating much simpler, but it does not completely eliminate the possibility of unobserved intermediate states. It remains possible that after the weakly voltage-dependent 'opening' transition in ILT, the channel undergoes a further rapid, voltage-independent transition between a narrow 'snug' (nonconductive) state and a wide, open state. In this alternative model, the snug state would permit the tight binding of cadmium and probably also the tight binding of quaternary ammonium blockers[17]. Although the open state in this model might be wide, its structure would be quite different from that of MthK to be consistent with the lock-open bridge. Our recovery data would be compatible with such a model only if a very specific coincidence (for both wild-type S4 and ILT channels) stabilizes the Cd^{2+}-bound snug state by an amount that almost exactly offsets the stability normally provided by coupling to the open state. A more serious challenge to this model is the observed rate of Cd^{2+} binding to 474C in the locked-open channels (Fig. 4). To explain this, we would need to suppose that the lock-open bridge decreases the occupancy of the snug state by no more than about sevenfold, which seems incompatible with the fact that the bridge reduces the closing rate by at least 1,000-fold (the dwell time of Cd^{2+} on the lock-open site is nearly a second, even at very negative voltages). Moreover, if the snug state provides the best fit for blockers like TEA and TBuA[17], then locking the channels in the open state ought to reduce the affinity, contrary to our observation (Fig. 2a). Taken together, the most straightforward interpretation of this body of functional data is that both metal bridges occur in the open state, and thus the structure of the Shaker inner helix in the open (and closed[15]) states is significantly different from that of the distant bacterial relatives KcsA and MthK (although no more different than is common within families of structurally related proteins).

The two bridges defined here provide strong constraints on the structure of the open state. Our proposed 'bent S6' model (centre, Fig. 5b) was derived by modifying the KcsA backbone to account for functional discrepancies with the KcsA structure[16,18]. The voltage-gated K^+ channel family has a highly conserved Pro-X-Pro motif in the middle of the S6, just at the bundle crossing in KcsA, which could serve as a helix-breaking sequence[19,20]. In our model, a kink in the KcsA helices was introduced at the Pro-Val-Pro (473–475) motif to bring V476C and H486 within distances appropriate for metal binding. This bent S6 model places both Cd^{2+} sites in acceptable binding positions simultaneously. Although we do not think that the open Shaker channel is likely to be quite so narrow (4–7 Å) as to allow optimum placement of the 474 cysteines for the binding of Cd^{2+}, a slightly larger opening (for example, ~8–9 Å) would permit hydrated K^+ ions (cross-section $\sim 6 \times 6$ Å)[21] and large quaternary ammonium blockers (such as TBuA or tetrahexylammonium; cross-sections of $\sim 4.5 \times 8$ Å) to enter the cavity[17,22], and would allow Cd^{2+} to bind with only minor flexibility (see ref. 23). The ability to assume the very narrow Cd^{2+}-binding position with equal ease from the open and closed states argues against a large motion at this position and for a constricted entrance to the cavity even in the open state.

The results indicate that at position V474 the intracellular entrance to the pore cavity of Shaker K^+ channels can be narrow in both states. The constriction of ion flow in the closed state is below this point, probably at position V478 (refs 16, 24). How, then, does the channel gate? Use of the conserved Pro-X-Pro as a flexible hinge or swivel could keep the upper S6 (and position 474) relatively still, but allow the lower half of the S6 to move, opening the pore by swivelling the blocking residues away from the central axis (Fig. 5). This is a different kind of movement than the large outward swing of

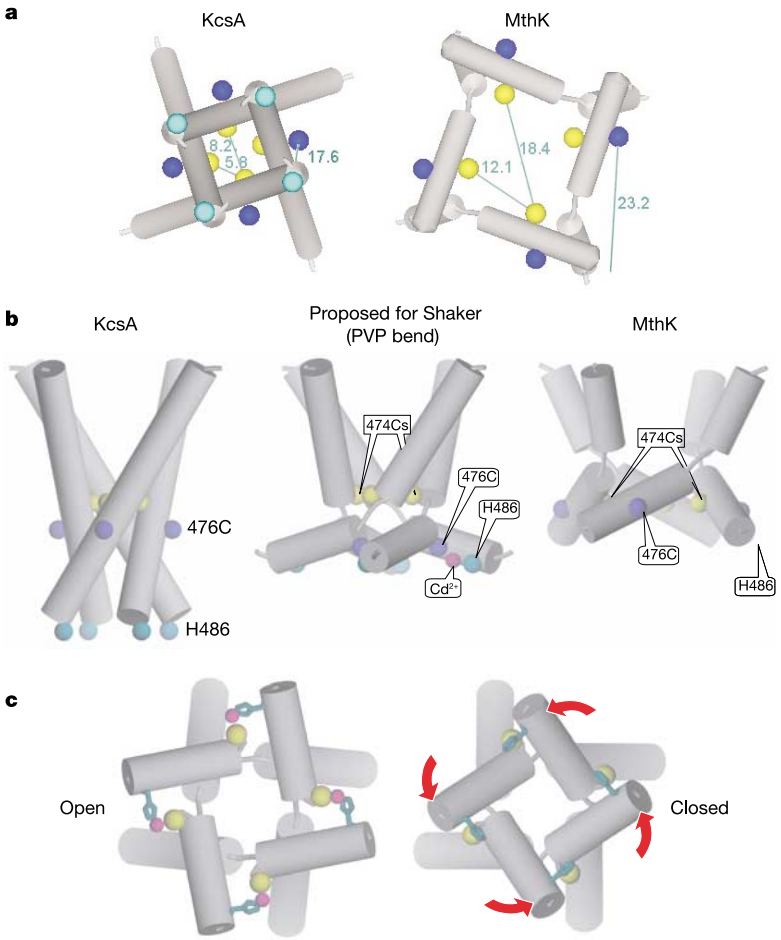

Figure 5 A comparison of the models of potassium channel gating. **a**, The distances between the positions equivalent to V474C (yellow) or between V476C (blue) and H486 (cyan) in the KcsA (left) or MthK (right) structures shown from the intracellular surface (position of the MthK 486-equivalent was estimated from a linear extension of the helix). **b**, The proposed Shaker pore structure (centre) is based on KcsA (left) but places a bend in the S6 at the conserved Pro-X-Pro motif (side view, colours as in **a** with Cd^{2+} in magenta). **c**, An intracellular view of a gating model based on the two Cd^{2+} bridges and previous constraints on the closed state[16].

helices that would result from a motion around the proposed hinge at the conserved glycine in the KcsA–MthK model of gating. In a combination of the two models, a similar opening motion might occur by swivelling at the glycine hinge with a fixed bend at the Pro-Val-Pro while maintaining the proximity of neighbouring V474C residues (that is, still pivoting around the Pro-Val-Pro).

Does the narrow opening of Shaker limit the maximum conductance of the channel? It has been proposed that the lower end of the S6 of Shaker contributes to a barrier for ion flow[10,11]. The MthK single-channel conductance[5] is ~220 pS, whereas Shaker conductance is about tenfold smaller, ~24 pS, in similar conditions[25]. The negative charges found in MthK and another large conductance channel, BK, account for only a small part of the difference in the conductance, only about twofold[26,27]. To account for the large difference in current flow, we suggest that a narrow opening in the class of smaller conductance channels such as Shaker places a diffusional barrier to ion conduction in the inner pore. Changing the geometry of the inner pore could modulate this conduction barrier, allowing for the tuning of single-channel conductance while maintaining strict ion preference in the selectivity filter. □

Methods

Molecular biology

Mutations were introduced by polymerase chain reaction (PCR) mutagenesis into our modified 'wild-type' cDNA[15], Shaker H4 Δ6-46 C301S C308S T449V. The ILT mutations (V369I, I372L and S376T) were transferred to our background by PCR generation of a fragment that was subcloned into the *Xba*I/*Bgl*II sites. Because the V476H mutant in a wild-type background opens at very negative voltages, we placed the mutation in an S4-LT (I372L, S376T) background[14] to shift gating into a more accessible voltage range. All mutations were confirmed by sequencing.

Recording and solutions

Channels were transiently expressed in HEK 293 cells by electroporation as described previously[15]; recordings were preformed 1–3 days after transfection. All experiments were conducted in inside-out patches pulled from identified transfected cells. The methods for rapid perfusion switches and electrophysiological recordings were as previously described[12], except in Fig. 4. In Fig. 4, a piezoelectric-driven solution-switching mechanism was used with a four-barrelled perfusion pipette[28]. Intracellular solutions contained (in mM) 160 KCl, 10 HEPES, 1 EGTA and 0.5 $MgCl_2$ (bath). Extracellular solutions contained (in mM) 60 KCl, 100 NaCl, 3 $CaCl_2$, 1 $MgCl_2$ and 10 HEPES, except in the experiments of Fig. 2b and Fig. 3, which contained 10 KCl and 150 NaCl.

When Cd^{2+} or Zn^{2+} were included, the EGTA was left out of the solution. The experimental cadmium and zinc concentrations are reported as the total concentration of metal. However, we used the chloride-buffer-corrected free concentration of Cd^{2+} to calculate the on rate constant in Fig. 4 (in the presence of 160 mM chloride ion, the calculated ratio of free $[Cd^{2+}]$ to total $[Cd^{2+}]$ is 0.13). For comparison, the previously reported on rate of Cd^{2+} to the single-mutant V474C channels[16] is $2.9 \pm 0.4 \times 10^6\ M^{-1}\,s^{-1}$ ($n = 4$) when corrected for buffering in the same way.

In the ILT mutants, there was evidence of a voltage-dependent block at positive voltages, which was alleviated by the removal of $MgCl_2$ from the intracellular solutions; the ILT experiments shown were carried out in the absence of internal $MgCl_2$.

The enhanced ball peptide we used in Fig. 2 has the sequence of the first 20 amino acids of Shaker with two mutations, E12K and E13K, to increase the positive charge[8]. DMPS stock solutions in water (50 mM) were made daily and kept on ice. Dilutions into intracellular solution were made just before each experiment.

Data analysis

Because channels continue to undergo slow inactivation when they are locked open, even

at very negative potentials, the lock-open currents were normalized to the current level in the control case for comparison. To estimate the $K_{1/2}$ of the blockers, the amount of block was estimated by isochronal comparison of the scaled traces.

In the single-channel recordings, the leak current and capacitative transients were subtracted with an idealized fit to a blank trace. Traces were filtered at 1 kHz, sampled at 2 kHz.

The rates of recovery of Shaker V474C from block by Cd^{2+} by DMPS were measured as the single exponential fit of the current as a function of the cumulative exposure at the test voltage. The test pulses were adjusted in length so that the time constant of recovery would be equal to at least two pulse durations. These single exponential rates were plotted versus voltage. Because of the large variation in the g-V midpoint for each experiment, the voltage of the recovery was corrected for the g-V midpoint of the individual experiment[13]: $V_{\text{corrected}} = V + (\overline{V_{\text{mid}}} - V_{\text{mid}})$. The average Boltzmann fit of the g-Vs is plotted.

Received 20 November 2003; accepted 4 March 2004; doi:10.1038/nature02468.

1. Jiang, Y. *et al.* The open pore conformation of potassium channels. *Nature* **417,** 523–526 (2002).
2. Doyle, D. A. *et al.* The structure of the potassium channel: molecular basis of K^+ conduction and selectivity. *Science* **280,** 69–77 (1998).
3. Kuo, A. *et al.* Crystal structure of the potassium channel KirBac1.1 in the closed state. *Science* **300,** 1922–1926 (2003).
4. Jiang, Y. *et al.* X-ray structure of a voltage-dependent K^+ channel. *Nature* **423,** 33–41 (2003).
5. Jiang, Y. *et al.* Crystal structure and mechanism of a calcium-gated potassium channel. *Nature* **417,** 515–522 (2002).
6. Heginbotham, L., Lu, Z., Abramson, T. & MacKinnon, R. Mutations in the K^+ channel signature sequence. *Biophys. J.* **66,** 1061–1067 (1994).
7. Holmgren, M., Shin, K. S. & Yellen, G. The activation gate of a voltage-gated K^+ channel can be trapped in the open state by an intersubunit metal bridge. *Neuron* **21,** 617–621 (1998).
8. Zagotta, W. N., Hoshi, T. & Aldrich, R. W. Restoration of inactivation in mutants of Shaker potassium channels by a peptide derived from ShB. *Science* **250,** 568–571 (1990).
9. Yellen, G., Jurman, M. E., Abramson, T. & MacKinnon, R. Mutations affecting internal TEA blockade identify the probable pore-forming region of a K^+ channel. *Science* **251,** 939–942 (1991).
10. Ding, S. & Horn, R. Tail end of the S6 segment: Role in permeation in Shaker potassium channels. *J. Gen. Physiol.* **120,** 87–97 (2002).
11. Lopez, G. A., Jan, Y. N. & Jan, L. Y. Evidence that the S6 segment of the Shaker voltage-gated K^+ channel comprises part of the pore. *Nature* **367,** 179–182 (1994).
12. Liu, Y., Holmgren, M., Jurman, M. E. & Yellen, G. Gated access to the pore of a voltage-dependent K^+ channel. *Neuron* **19,** 175–184 (1997).
13. Smith-Maxwell, C. J., Ledwell, J. L. & Aldrich, R. W. Role of the S4 in cooperativity of voltage-dependent potassium channel activation. *J. Gen. Physiol.* **111,** 399–420 (1998).
14. Smith-Maxwell, C. J., Ledwell, J. L. & Aldrich, R. W. Uncharged S4 residues and cooperativity in voltage-dependent potassium channel activation. *J. Gen. Physiol.* **111,** 421–439 (1998).
15. Ledwell, J. L. & Aldrich, R. W. Mutations in the S4 region isolate the final voltage-dependent cooperative step in potassium channel activation. *J. Gen. Physiol.* **113,** 389–414 (1999).
16. del Camino, D. & Yellen, G. Tight steric closure at the intracellular activation gate of a voltage-gated K^+ channel. *Neuron* **32,** 649–656 (2001).
17. Zhou, M., Morais-Cabral, J. H., Mann, S. & MacKinnon, R. Potassium channel receptor site for the inactivation gate and quaternary amine inhibitors. *Nature* **411,** 657–661 (2001).
18. del Camino, D., Holmgren, M., Liu, Y. & Yellen, G. Blocker protection in the pore of a voltage-gated K^+ channel and its structural implications. *Nature* **403,** 321–325 (2000).
19. Tieleman, D. P., Shrivastava, I. H., Ulmschneider, M. R. & Sansom, M. S. Proline-induced hinges in transmembrane helices: possible roles in ion channel gating. *Proteins* **44,** 63–72 (2001).
20. Bright, J. N., Shrivastava, I. H., Cordes, F. S. & Sansom, M. S. Conformational dynamics of helix S6 from Shaker potassium channel: simulation studies. *Biopolymers* **64,** 303–313 (2002).
21. Zhou, Y., Morais-Cabral, J. H., Kaufman, A. & MacKinnon, R. Chemistry of ion coordination and hydration revealed by a K^+ channel-Fab complex at 2.0 Å resolution. *Nature* **414,** 43–48 (2001).
22. Holmgren, M., Smith, P. L. & Yellen, G. Trapping of organic blockers by closing of voltage-dependent K^+ channels: evidence for a trap door mechanism of activation gating. *J. Gen. Physiol.* **109,** 527–535 (1997).
23. Loussouarn, G., Phillips, L. R., Masia, R., Rose, T. & Nichols, C. G. Flexibility of the Kir6.2 inward rectifier K^+ channel pore. *Proc. Natl Acad. Sci. USA* **98,** 4227–4232 (2001).
24. Hackos, D. H., Chang, T. H. & Swartz, K. J. Scanning the intracellular S6 activation gate in the Shaker K^+ channel. *J. Gen. Physiol.* **119,** 521–532 (2002).
25. Isacoff, E. Y., Jan, Y. N. & Jan, L. Y. Putative receptor for the cytoplasmic inactivation gate in the Shaker K^+ channel. *Nature* **353,** 86–90 (1991).
26. Nimigean, C. M., Chappie, J. S. & Miller, C. Electrostatic tuning of ion conductance in potassium channels. *Biochemistry* **42,** 9263–9268 (2003).
27. Brelidze, T. I., Niu, X & Magleby, K. L. A ring of eight conserved negatively charged amino acids doubles the conductance of BK channels and prevents inward rectification. *Proc. Natl Acad. Sci. USA* **100,** 9017–9022 (2003).
28. Forman, S. A. A hydrophobic photolabel inhibits nicotinic acetylcholine receptors via open-channel block following a slow step. *Biochemistry* **38,** 14559–14564 (1999).

Acknowledgements We thank M. Kanevsky for characterizing the charge movement for ILT 474C and S. Forman for allowing us to use his perfusion setup. We are also grateful to B. Bean and to the members of the Yellen laboratory for helpful discussions, and to T. Abramson for her expert help with transfections. This work was supported by a grant from the NIH/NINDS to G.Y.

Competing interests statement The authors declare that they have no competing financial interests.

Correspondence and requests for materials should be addressed to G.Y. (gary_yellen@hms.harvard.edu).

Programmed population control by cell–cell communication and regulated killing

Lingchong You[1], Robert Sidney Cox III[2], Ron Weiss[3] & Frances H. Arnold[1]

[1]*Division of Chemistry and Chemical Engineering and* [2]*Division of Biology, California Institute of Technology, Pasadena, California 91125, USA*
[3]*Departments of Electrical Engineering and Molecular Biology, Princeton University, Princeton, New Jersey 08544, USA*

***De novo* engineering of gene circuits inside cells is extremely difficult[1–9], and efforts to realize predictable and robust performance must deal with noise in gene expression and variation in phenotypes between cells[10–12]. Here we demonstrate that by coupling gene expression to cell survival and death using cell–cell communication, we can programme the dynamics of a population despite variability in the behaviour of individual cells. Specifically, we have built and characterized a 'population control' circuit that autonomously regulates the density of an *Escherichia coli* population. The cell density is broadcasted and detected by elements from a bacterial quorum-sensing system[13,14], which in turn regulate the death rate. As predicted by a simple mathematical model, the circuit can set a stable steady state in terms of cell density and gene expression that is easily tunable by varying the stability of the cell–cell communication signal. This circuit incorporates a mechanism for programmed death in response to changes in the environment, and allows us to probe the design principles of its more complex natural counterparts.**

Our circuit (Fig. 1a) programmes a bacterial population to maintain a cell density that is lower than the limits imposed by the environment (for example, by nutrient supply). The LuxI protein of the well-characterized LuxI/LuxR system from the marine bacterium *Vibrio fischeri*[13,14] synthesizes a small, diffusible acyl-homoserine lactone (AHL) signalling molecule. The AHL accumulates in the experimental medium and inside the cells as the cell density increases. At sufficiently high concentrations, it binds and activates the LuxR transcriptional regulator, which in turn induces the expression of a killer gene (*E*) under the control of a *luxI* promoter (p_{luxI})[15]. Sufficiently high levels of the killer protein cause cell death.

We implemented the circuit using a two-plasmid system (Fig. 1b), where pLuxRI2 expresses LuxI and LuxR upon induction by isopropyl-β-D-thiogalactopyranoside (IPTG), and p*lux*CcdB3 responds to activated LuxR (at sufficiently high cell density) and causes cell death. The *lacZα–ccdB* killer gene codes for a fusion protein of LacZα and CcdB. The LacZα portion of the fusion protein retains the ability to complement LacZΔM15 in appropriate cell strains (for example, Top10F′ cells), allowing the measurement of fusion protein levels using a LacZ assay (see Methods). The CcdB portion retains the toxicity of native CcdB, which kills susceptible cells by poisoning the DNA gyrase complex[16].

A simple mathematical model predicted that the system would reach a stable cell density for all realistic parameter values (see Methods), although it might go through damped oscillations while approaching the steady state. Experiments confirmed our predictions. Figure 2a shows the growth of Top10F′ cells containing the population-control circuit at pH 7.0. As anticipated, the uninduced culture (circuit OFF) grew exponentially and reached the stationary phase upon nutrient exhaustion. The induced culture (circuit ON) grew almost identically, until its density reached a threshold (at 7 h). It then deviated sharply from the OFF culture and briefly went through a damped oscillation (between 7 h and 24 h) of at least one cycle before reaching a steady-state density about ten times lower than that of the OFF culture. The measured peak density (at 10 h)